Physics of the Dark Universe 26 (2019) 100362

Contents lists available at ScienceDirect

Physics of the Dark Universe

journal homepage: www.elsevier.com/locate/dark

Effective approximation of electromagnetism for axion haloscope searches

Younggeun Kim [a,b], Dongok Kim [a,b], Junu Jeong [a,b], Jinsu Kim [a,b], Yun Chang Shin [a,*], Yannis K. Semertzidis [a,b]

[a] Center for Axion and Precision Physics Research, Institue for Basic Science, Daejeon, 34051, South Korea
[b] Department of Physics, KAIST, Daejeon, 34141, South Korea

ARTICLE INFO

Article history:
Received 31 January 2019
Received in revised form 11 July 2019
Accepted 26 July 2019

ABSTRACT

The incorporation of axion-photon interaction into the classical Maxwell's equations has provided insights for axion searches with microwave photons. In addition to current leading axion haloscope searches with resonant cavities for axions in resonance regime (10^{-6}eV $< m_a <$ 10^{-4}eV), new proposed experiments also make the most of the Maxwell's equations to detect an induced electromagnetic field from the axion-photon interaction in long wavelength regime ($m_a \ll 10^{-6}$eV). In this paper, we apply an effective approximation to the Maxwell's equations to get a correct form of Maxwell's equations only for the induced fields. We rigorously solve the Maxwell's equations for the induced fields to get a close form of electromagnetic fields under various experimental conditions in the axion resonance regime. We attempt to get the electromagnetic field in the long wavelength regime, directly from the solutions in the resonance regime, by taking the long wavelength limit. Axion to photon conversion power in the axion resonance regime was also examined not only for on-resonance frequency, but also for off-resonance frequency region. This would provide information to estimate the conversion power even in off-resonant region of the cavity modes that can be applied for the axion searches.

1. Introduction

Axions are hypothetical particles suggested by the Peccei-Quinn (PQ) theory as a solution of the strong CP problem in the Standard Model [1]. Phenomenological searches indicate that axions could be invisible because of their weak coupling with matter [2,3]. If axions are indeed invisible, they could play an important role in the composition of dark matter and be ubiquitous in our Universe. This invisibility of the axion has been described by two different axion models, the KSVZ and DFSZ [4–7].

In addition to the very weak coupling of axions with particles from the Standard Model, their interaction with electromagnetic fields is also known to be very weak [8,9]. The interaction of an axion with an electromagnetic field is governed by allowing coupling of the axion to the electromagnetic field expressed as

$$a\mathbf{E}\cdot\mathbf{B} \propto -aF_{\mu\nu}\tilde{F}^{\mu\nu}. \tag{1}$$

This coupling results in a conversion of axions into two photons via inverse Primakoff effect proposed by Sikivie [9,10]. Most of the successful experiments searching for axions are based on this axion-photon interaction with an assumption of axions as halo dark matter, which are accordingly called axion haloscope searches [10,11]. This experimental scheme is to detect a very weak trace of dark matter axions converted into microwave photons in the presence of a static magnetic field. Since they are dealing with the electromagnetic fields, the axion haloscope experiments can be described in the framework of classical Maxwell's equations. However, the classical Maxwell's equations need to be modified in order to include the axion-photon interaction [12–14].

The effective Lagrangian describing the axion electromagnetic interaction can be derived in SI units as

$$\mathcal{L}_{0+a} = \mathcal{L}_0+\mathcal{L}_a+\mathcal{L}_U = -\frac{1}{4\mu_0}F^{\mu\nu}F_{\mu\nu}+\frac{g_{a\gamma\gamma}}{4\mu_0}aF^{\mu\nu}\tilde{F}_{\mu\nu}-A_\mu J_e^\mu+\mathcal{L}_U, \tag{2}$$

where $\mathcal{L}_0 = -\frac{1}{4\mu_0}F^{\mu\nu}F_{\mu\nu} - A_\mu J_e^\mu$ is the classical EM Lagrangian, $\mathcal{L}_U = \frac{1}{2}(\partial^\mu a)(\partial_\mu a) - U(a) = \frac{1}{2}(\partial^\mu a)(\partial_\mu a) - \frac{1}{2}\omega_a^2 a^2$ is the axion Lagrangian with a potential $U(a)$, and the axion interaction term

$$\mathcal{L}_a = \frac{g_{a\gamma\gamma}}{4\mu_0}aF^{\mu\nu}\tilde{F}_{\mu\nu} = -\frac{g_{a\gamma\gamma}}{\mu_0 c}a\mathbf{E}\cdot\mathbf{B}. \tag{3}$$

* Corresponding author at: Center for Axion and Precision Physics Research, Institute for Basic Science, Daejeon, 34051, South Korea.
E-mail address: yunshin@ibs.re.kr (Y.C. Shin).

https://doi.org/10.1016/j.dark.2019.100362
2212-6864/

The two-photon coupling to an axion field, $g_{a\gamma\gamma}$, is defined in units of GeV^{-1} as

$$g_{a\gamma\gamma} = \frac{\alpha_{EM}}{2\pi f_a} c_{a\gamma\gamma}, \tag{4}$$

where $\alpha_{EM} \approx 1/137$ is the fine structure constant and f_a is the axion decay constant in units of GeV [2]. $c_{a\gamma\gamma}$ is the dimensionless coupling, which is model dependent as $c_{a\gamma\gamma} = -1.92$ (KSVZ), or $c_{a\gamma\gamma} = 0.75$ (DFSZ) [4–7]. For a QCD axion, the $g_{a\gamma\gamma}$ is defined by the breaking scale f_a of the Peccei-Quinn (PQ) symmetry. For a generic axion like particle (ALP), the coupling $g_{a\gamma\gamma}$ is treated as a free parameter which is assumed to be much smaller than one for the QCD axion in certain ALP models [15].

In both cases, Maxwell's equations with the axion-photon interaction can be derived from the Lagrangian written in Eq. (3) with the Bianchi Identity as follows,

$$\nabla \cdot \left(\mathbf{E} - c g_{a\gamma\gamma} a \mathbf{B}\right) = \frac{\rho_e}{\varepsilon}, \tag{5a}$$

$$\nabla \cdot \mathbf{B} = 0, \tag{5b}$$

$$\nabla \times \mathbf{E} = -\frac{\partial \mathbf{B}}{\partial t}, \tag{5c}$$

$$\nabla \times \left(c\mathbf{B} + g_{a\gamma\gamma} a \mathbf{E}\right) = \frac{1}{c}\frac{\partial}{\partial t}\left(\mathbf{E} - c g_{a\gamma\gamma} a \mathbf{B}\right) + c\mu \mathbf{J}_e. \tag{5d}$$

Many ongoing experimental searches for axions from the Sikivie method are all based on the Maxwell's equations in Eq. (5) [9,10].

Axion haloscope searches from a resonant cavity are looking for electromagnetic fields generated by the axion in the resonant cavity under a static homogenous magnetic field $\mathbf{B}_{\text{ext}}$ [10]. Since the cavity haloscope method for axion searches was first introduced [16], the experimental condition for the cavity haloscope has been considered to be a cylindrical cavity placed in a static homogeneous magnetic field in the longitudinal direction $\mathbf{B}_{\text{ext}} = \mathrm{B}_0\hat{z}$. But, as a toroidal magnetic field also has been proposed for the axion searches [17], the static homogeneous magnetic field would have a more generalized condition with $\nabla \times \mathbf{B}_{\text{ext}} = 0$, and thus satisfy all types of static homogeneous magnetic field.

Non-relativistic axion dark matter has a velocity distribution on the scale of the virial velocity of a local dark matter halo $v_{\text{vir}} = \xi c$ with, $\xi \approx 10^{-3}$ [2]. The velocity distribution also results in the coherent length of axion dark matter $\lambda_{\text{coh}} = \hbar/m_a \xi c = 1000\lambda_a$, where λ_a is the Compton wavelength corresponding to the axion mass. For most cavity haloscope experiments, the size of the static magnetic fields is still well below that of the coherent length of the axion. Therefore, the spatial dependence of the axion field can be ignored at laboratory scale ($\nabla a \approx 0$).

The axion field is considered as a coherently oscillating field $a(t) = a_0 e^{-i\omega_a t}$ where ω_a is the oscillating frequency corresponding to axion mass m_a [2,10]. The amplitude of the axion field can be $a_0 = \frac{\sqrt{2\rho_{\text{DM}}\hbar^3/c}}{m_a}$ where ρ_{DM} is the local galactic dark matter density as $\rho_{\text{DM}} \approx 0.3$ GeV/cm^3 [18].

In addition, there is no electric charge and the current density in the cavity: $\rho_e = 0$ and $J_e = 0$. Normally, no external electric field is applied in the region as well $\mathbf{E}_{\text{ext}} = 0$.

Recently, McAllister et al. [19] presented a solution of electromagnetic fields induced by the axion-photon conversion in a long cylindrical, solenoidal external magnetic field. These fields were given as a solution of Maxwell's equations in Eq. (1) as

$$\mathbf{E}_a = -c g_{a\gamma\gamma} a \mathrm{B}_0 \hat{z}, \tag{6a}$$

$$\mathbf{B}_a = -\frac{g_{a\gamma\gamma}}{2c} r \mathrm{B}_0 \frac{\partial a}{\partial t}\hat{\phi}. \tag{6b}$$

They estimated the complete expression of the electromagnetic form factor for cavity haloscope experiments based on this set of solutions. They also proposed a new experimental idea to search for axions in a mass range below 10^{-6} eV using a broadband scheme [20]. The basic concept of this idea was to detect the electric field estimated in Eq. (6a).

However, it is conspicuous that Eqs. (6a) and (6b) are not compatible solutions for the axion-photon interaction in the axion resonance regime where the Compton wavelength corresponding to the axion mass (10^{-6} eV $< m_a < 10^{-4}$ eV) is similar to the typical size of the external magnetic field ($\lambda_a \approx R$) in current experiments with resonant cavities. Eq. (6b) might be effective in a long wavelength regime of axions where the Compton wavelength corresponding to the axion mass ($m_a \ll 10^{-6}$ eV) is much longer than the typical size of the external magnetic field ($\lambda_a \gg R$). But there is still a lack of compatibility between $\mathbf{E}_a$ and $\mathbf{B}_a$ even in the long wavelength regime. This can be clearly checked by substituting Eqs. (6a) and (6b) back into the Maxwell's equations.

As a matter of fact, the induced magnetic field in Eq. (6b) could be derived in the long wavelength regime when assuming a quasi-magnetostatic condition, in which an electric current density $\mathbf{J}_a = -\sqrt{\epsilon_0/\mu_0} g_{a\gamma\gamma} \dot{a} \mathbf{B}_{\text{ext}}$ produces the magnetic field in Eq. (5) via $\nabla \times \mathbf{B}_a = \mathbf{J}_a$ [21]. Thereby, a broadband axion search would be possible by detecting and amplifying the effective magnetic field with an LC circuit and a sensitive magnetometer. A similar detection concept has been also proposed to search for the axion-induced oscillating magnetic field, $\mathbf{B}_a$, generated by a toroidal magnetic field with a superconducting pickup loop in the center of a toroidal magnet [22]. In the resonance regime, the solution of electromagnetic fields generated from the axion-photon interaction could be evaluated by solving the Maxwell's equations rigorously. But it is still necessary to set a boundary condition defined by the geometry of the conductive cavity, which is required to enhance the conversion signal, in the static magnetic field.

Moreover, in both the resonance ($\lambda_a \approx R$) and long wavelength ($\lambda_a \gg R$) regimes, the Maxwell's equations in Eq. (5) needs to be rearranged with the order of the axion-photon coupling, $g_{a\gamma\gamma}$, to deal only with the electromagnetic field that is generated from the axion-photon interaction. We will refer to this field as the reacted field from now on. Both of the reacted field and the external field appear in the Maxwell's equations in Eq. (5). But they are not clearly distinguished from each other. We think this may cause the fallacy in the interpretation of the Maxwell's equations, as in Eq. (6).

In this paper, we apply an effective approximation to obtain decoupled Maxwell's equations only for the reacted electromagnetic field. Throughout the paper, we will refer to it as the decoupled Maxwell's equations. This will be described in Section 2. We will show the solution of the decoupled Maxwell's equations in the resonant regime in Section 3. The solution of the electromagnetic field in the resonant regime was precisely evaluated by solving the decoupled Maxwell's equations with relevant boundary conditions from the conductive cavity. In Section 4, we also show that the reacted electromagnetic field in the long wavelength regime can be derived from the solution estimated in the resonance regime by taking a long wavelength limit. From the decoupled Maxwell's equations, we derive an expression of axion conversion power in the axion resonance regime considering the effect of the energy difference between the electric field and the magnetic field.

2. Separation of maxwell's equations

2.1. Incomplete relationship of the fields solution

In the Maxwell's equations in Eq. (5), if one treats the electromagnetic field $\mathbf{E}$ and $\mathbf{B}$ as the external electromagnetic fields, $\mathbf{E}_{\text{ext}}$ and $\mathbf{B}_{\text{ext}}$, respectively, Eq. (5d) becomes

$$\nabla \times \mathbf{B}_{\text{ext}} = -\frac{g_{a\gamma\gamma}}{c} \mathbf{B}_{\text{ext}} \frac{\partial a}{\partial t}. \tag{7}$$

While the boundary condition constrains $\nabla \times \mathbf{B}_{\rm ext} = 0$ on the left side of Eq. (7), the right side does not intuitively become zero because of the axion-photon interaction term.

In Refs. [19,23], this problem was avoided by forcing the non-zero term in Eq. (7) as a relationship of new fields $\mathbf{E}_a$ and $\mathbf{B}_a$ as

$$\nabla \times \mathbf{B}_a = -\frac{g_{a\gamma\gamma}}{c}\mathbf{B}_{\rm ext}\frac{\partial a}{\partial t} = \frac{1}{c^2}\frac{\partial \mathbf{E}_a}{\partial t}, \tag{8}$$

where $\mathbf{E}_a$ and $\mathbf{B}_a$ are the electric and magnetic field components of the photons produced via the axion-photon interaction. At the same time, the other relationship between $\mathbf{E}_a$ and $\mathbf{B}_a$ was defined in Ref. [19,23] from Eq. (7) with cavity haloscope conditions as

$$\nabla \times \mathbf{E}_a = -\frac{\partial \mathbf{B}_a}{\partial t}. \tag{9}$$

Eq. (9) is indeed the Maxwell-Faraday equation which is a generalization of Faraday's law. Dynamical electromagnetic fields defined in any space from given boundary conditions have to satisfy this relationship. In Refs. [19,23], the $\mathbf{E}_a$ was estimated from the right side of the relationship in Eq. (8) as

$$-\frac{g_{a\gamma\gamma}}{c}\mathbf{B}_{\rm ext}\frac{\partial a}{\partial t} = \frac{1}{c^2}\frac{\partial \mathbf{E}_a}{\partial t}. \tag{10}$$

The axion induced electric field $\mathbf{E}_a$ was obtained from Eq. (10) as

$$\mathbf{E}_a = -cg_{a\gamma\gamma}a\mathbf{B}_{\rm ext} + \mathbf{f}(\mathbf{r}), \tag{11}$$

where the function $\mathbf{f}(\mathbf{r})$ can have only position dependence. At the same time, $\mathbf{B}_a$ in Refs. [19,23] was estimated by applying Stokes' theorem in the left side of the relationship in Eq. (8) as follows:

$$\int_{\mathcal{A}} (\nabla \times \mathbf{B}_a)\cdot d\mathbf{A} = \oint_{\partial\mathcal{A}} \mathbf{B}_a \cdot d\mathbf{l} = -\frac{g_{a\gamma\gamma}}{c}\dot{a}\mathcal{A}\mathbf{B}_{\rm ext}, \tag{12}$$

where $\mathcal{A}$ is the area to be integrated, and we assume a uniform external magnetic field $\mathbf{B}_{\rm ext} = \mathrm{B}_0\hat{z}$. If we consider a certain geometry which has a rotational symmetry along the z axis such as a cylindrical cavity, $\mathbf{B}_a$ can be estimated from Eq. (12) as

$$\mathbf{B}_a = -\frac{g_{a\gamma\gamma}}{2c}r\mathrm{B}_0\dot{a}\hat{\phi}. \tag{13}$$

If the $\mathbf{E}_a$ and $\mathbf{B}_a$ are compatible solutions, they should satisfy the Maxwell-Faraday's law in Eq. (9). To check it, substituting Eqs. (11) and (13) back in Eq. (9) becomes

$$\nabla \times \mathbf{E}_a = \nabla \times \left(-cg_{a\gamma\gamma}a\mathbf{B}_{\rm ext} + \mathbf{f}(\mathbf{r})\right) = -\frac{g_{a\gamma\gamma}}{2c}r\mathrm{B}_0\ddot{a}\hat{\phi}. \tag{14}$$

Since we assume that $\mathbf{f}$ is a function of only $\mathbf{r}$, no solution for $\mathbf{f}(\mathbf{r})$ is possible to satisfy Eq. (14) unless $\ddot{a} = 0$. Otherwise, these solutions for an electromagnetic field obtained from Eq. (8) do not explicitly satisfy Maxwell-Faraday's law. As we have shown, Eq. (8) possesses a fundamentally incomplete relationship. Therefore, one cannot evaluate electromagnetic fields directly from both relationships in Eq. (8).

2.2. Decoupling of reacted fields

We think this is because the reacted electromagnetic field was not clearly decoupled from the external electromagnetic field applied for the axion interaction in the Maxwell's equations. For decoupling of fields, we applied an effective approximation into the Maxwell's equations in Eq. (5) [24,25]. By assuming that the axion-photon interaction slightly perturbs the electromagnetic field, we can apply the following relationships into the electromagnetic field as

$$\mathbf{E} = \sum_m (g_{a\gamma\gamma})^m \mathbf{E}_m = \mathbf{E}_0 + g_{a\gamma\gamma}\mathbf{E}_1 + g_{a\gamma\gamma}^2\mathbf{E}_2 + \cdot\cdot, \tag{15a}$$

$$\mathbf{B} = \sum_m (g_{a\gamma\gamma})^m \mathbf{B}_m = \mathbf{B}_0 + g_{a\gamma\gamma}\mathbf{B}_1 + g_{a\gamma\gamma}^2\mathbf{B}_2 + \cdot\cdot. \tag{15b}$$

Since $g_{a\gamma\gamma}$ is roughly $\sim 10^{-8}$ GeV^{-1} or less both for QCD axion and ALP cases, the higher order terms are ignored and only the leading and first order terms can be considered as

$$\mathbf{E} \simeq \mathbf{E}_0 + g_{a\gamma\gamma}\mathbf{E}_1, \tag{16a}$$

$$\mathbf{B} \simeq \mathbf{B}_0 + g_{a\gamma\gamma}\mathbf{B}_1. \tag{16b}$$

If we input the field relations in Eq. (16) into the Maxwell's equations in Eq. (5), and ignore the $g_{a\gamma\gamma}{}^2$ terms again, the set of equations is reduced as

$$\nabla \cdot \left(\mathbf{E}_0 + g_{a\gamma\gamma}\mathbf{E}_1 - cg_{a\gamma\gamma}a\mathbf{B}_0\right) = \rho_e/\epsilon_0, \tag{17a}$$

$$\nabla \cdot \left(\mathbf{B}_0 + g_{a\gamma\gamma}\mathbf{B}_1\right) = 0, \tag{17b}$$

$$\nabla \times \left(\mathbf{E}_0 + g_{a\gamma\gamma}\mathbf{E}_1\right) = -\frac{\partial}{\partial t}\left(\mathbf{B}_0 + g_{a\gamma\gamma}\mathbf{B}_1\right), \tag{17c}$$

$$\nabla \times (\mathbf{B}_0 + g_{a\gamma\gamma}\mathbf{B}_1 + \frac{1}{c}g_{a\gamma\gamma}a\mathbf{E}_0) =$$
$$\frac{1}{c^2}\frac{\partial}{\partial t}(\mathbf{E}_0 + g_{a\gamma\gamma}\mathbf{E}_1 - cg_{a\gamma\gamma}a\mathbf{B}_0) + \mu_0\mathbf{J}_e. \tag{17d}$$

Now one can assume a certain space filled with the external electromagnetic field, $\mathbf{E}_0$ and $\mathbf{B}_0$. If there is no axion, there is no axion-photon interaction. Therefore, the total electromagnetic field in the space will still remain $\mathbf{E} = \mathbf{E}_0$ and $\mathbf{B} = \mathbf{B}_0$. In this case, none of the terms in $g_{a\gamma\gamma}$ generated from the axion interaction in Eq. (17) survive. Then, Eq. (17) will be reduced into Maxwell's equations describing $\mathbf{E}_0$ and $\mathbf{B}_0$ only.

However, if there are interactions between the external electromagnetic field and axions through the axion-photon interaction term, a reacted electromagnetic field, $\mathbf{E}_{\rm r}$, $\mathbf{B}_{\rm r}$, will be generated. Therefore, the total electric and magnetic fields $\mathbf{E}$ and $\mathbf{B}$ in the space are slightly different from the applied external fields $\mathbf{E}_0$ and $\mathbf{B}_0$. In this case, the total fields can be expressed as a superposition of the original fields $\mathbf{E}_0$, $\mathbf{B}_0$ and the reacted fields from the axion-interaction term, $\mathbf{E}_{\rm r}$, $\mathbf{B}_{\rm r}$ as

$$\mathbf{E} = \mathbf{E}_0 + \mathbf{E}_{\rm r}, \tag{18a}$$

$$\mathbf{B} = \mathbf{B}_0 + \mathbf{B}_{\rm r}. \tag{18b}$$

By recalling Eq. (16), one can set the relationships of the reacted fields as

$$\mathbf{E}_{\rm r} = g_{a\gamma\gamma}\mathbf{E}_1, \tag{19a}$$

$$\mathbf{B}_{\rm r} = g_{a\gamma\gamma}\mathbf{B}_1. \tag{19b}$$

Using above relationship, we can separate the Maxwell's equations into two parts. One is only for the external fields and the other is only for the reacted field. The Maxwell's equations only for the external electromagnetic fields become

$$\nabla \cdot \mathbf{E}_0 = \rho_e/\epsilon_0, \tag{20a}$$

$$\nabla \cdot \mathbf{B}_0 = 0, \tag{20b}$$

$$\nabla \times \mathbf{E}_0 = -\frac{\partial}{\partial t}\mathbf{B}_0, \tag{20c}$$

$$\nabla \times \mathbf{B}_0 = \frac{1}{c^2}\frac{\partial}{\partial t}\mathbf{E}_0 + \mu_0\mathbf{J}_e. \tag{20d}$$

And Maxwell's equations only for the reacted fields become

$$\nabla \cdot \left(\mathbf{E}_{\rm r} - cg_{a\gamma\gamma}a\mathbf{B}_0\right) = 0, \tag{21a}$$

$$\nabla \cdot \mathbf{B}_{\rm r} = 0, \tag{21b}$$

$$\nabla \times \mathbf{E}_{\rm r} = -\frac{\partial \mathbf{B}_{\rm r}}{\partial t}, \tag{21c}$$

$$\nabla \times \left(\mathbf{B}_{\rm r} + \frac{1}{c}g_{a\gamma\gamma}a\mathbf{E}_0\right) = \frac{1}{c^2}\frac{\partial}{\partial t}(\mathbf{E}_{\rm r} - cg_{a\gamma\gamma}a\mathbf{B}_0). \tag{21d}$$

As shown in Eqs. (20) and (21), Maxwell's equations can be clearly separated into two parts. Both of Eqs. (20) and (21) can be exactly solved. Since the reacted fields are the main interest for most axion haloscope experiments, we will show our estimation of the reacted fields from the decoupled Maxwell's equations in Eq. (21) in the following sections. We will also show that the field solution getting from the decoupled the Maxwell's equations is in distinct contrast to the result from McAllister in Eq. (6) [19] in next section.

3. Electromagnetic field in various axion wavelength limit

Now, we can estimate the reacted electromagnetic fields in various experimental conditions from the decoupled Maxwell's equations in Eq. (21). We can roughly define two distinct axion mass regimes for many different experiments searching for axions. The first one is the axion resonance regime where the Compton wavelength corresponding to the axion mass λ_a is compatible with the size R_0 of the static homogeneous external field, and correspondingly a conductive boundary applied for the resonance, as $\lambda_a \approx R_0$. Most of the axion haloscope experiments with a resonant cavity approximately meet in this regime since they are dealing with axions in a mass range 10^{-6} eV $< m_a < 10^{-4}$ eV with the size of the static magnetic field roughly less than $\sim 1m$. In this regime, the reacted electromagnetic field would resonate in cavity modes placed in the external magnetic field and the signal could be resonantly enhanced with the cavity.

If the axion mass becomes very light ($m_a \ll 10^{-6}$ eV), the Compton wavelength corresponding to the axion mass λ_a would be much larger than the typical size of the static magnetic fields ($\lambda_a \gg R_0$). In this long wavelength regime, the reacted electromagnetic field would behave in a very different way from one in the resonance regime. Quasi-static conditions can be assumed so that the reacted field with the longer wavelength would flow out even across the boundary instead of resonating in the boundary. But it is still possible to detect the reacted fields with inductive magnetometer sensors because they still slowly oscillate with the axion frequency [21,22].

3.1. Resonance regime in a cylindrical cavity

Currently, ADMX, HAYSTAC, and CULTASK are the leading experiments looking for axions with resonant cavities in an axion mass range 10^{-6} eV $< m_a < 10^{-4}$ eV [26–29]. Although different in size, they all make use of a cavity of cylindrical geometry as the conductive boundary in a static external magnetic field. Therefore, all these experiments are in the resonance regime ($\lambda_a \approx R_0$). We first evaluated the reacted electromagnetic field in this regime from the decoupled Maxwell's equations in Eq. (21). We assumed an infinitely long solenoidal magnet and infinitely long cylindrical cavity with finite radius R_0 to allow a simple solution in the cylindrical coordinate as shown in Fig. 1. A cylindrical DC magnetic field ($\mathbf{B}_{\rm ext} = \mathrm{B}_0\hat{z}$) from the solenoidal magnet was assumed to be applied only inside the cavity along the longitudinal axis of the cavity.

From the cavity haloscope condition, the decoupled Maxwell's equations for the reacted electromagnetic fields are given as

$$\nabla \cdot \mathbf{E}_{\rm r} = 0, \tag{22a}$$

$$\nabla \cdot \mathbf{B}_{\rm r} = 0, \tag{22b}$$

$$\nabla \times \mathbf{E}_{\rm r} = -\frac{\partial \mathbf{B}_{\rm r}}{\partial t}, \tag{22c}$$

$$\nabla \times \mathbf{B}_{\rm r} = \frac{1}{c^2}\frac{\partial}{\partial t}(\mathbf{E}_{\rm r} - cg_{a\gamma\gamma}a\mathbf{B}_{\rm ext}), \tag{22d}$$

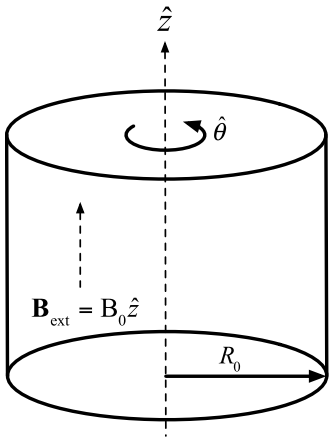

Fig. 1. Cylindrical cavity with radius R_0. The static magnetic field $\mathbf{B}_{\rm ext}$ has been applied inside the cavity along the longitudinal direction as $\mathbf{B}_{\rm ext} = \mathrm{B}_0\hat{z}$.

where $\mathbf{E}_{\rm r}$ and $\mathbf{B}_{\rm r}$ denote the reacted electric and magnetic fields, respectively. A set of wave equations for the reacted fields can be derived from Eq. (22) as,

$$\nabla^2\mathbf{E}_{\rm r} = \frac{\partial^2}{c^2\partial t^2}\mathbf{E}_{\rm r} - \frac{g_{a\gamma\gamma}}{c}\mathbf{B}_{\rm ext}\frac{\partial^2}{\partial t^2}a(t), \tag{23a}$$

$$\nabla^2\mathbf{B}_{\rm r} = \frac{\partial^2}{c^2\partial t^2}\mathbf{B}_{\rm r}. \tag{23b}$$

To solve the wave equations in Eq. (23) for the resonant cavity, it is necessary to define an additional boundary condition set by the size of the conductive cavity, which all current cavity haloscope experiments take on. We consider two distinct cases for the conductivity of the cavity. One has the perfect electric conductivity (PEC) for the ideal case and the other has finite conductivity for a more realistic case. For simplicity, the size of the static magnetic field is assumed to be the same as the size of the cavity, R_0.

In the ideal case of PEC, Eq. (23a) can be solved in a straightforward way. The solution for the electric field can be separated into a homogeneous solution $\mathbf{E}_{\rm r}^h$ and special solution $\mathbf{E}_{\rm r}^s$ as $\mathbf{E}_{\rm r} = \mathbf{E}_{\rm r}^h + \mathbf{E}_{\rm r}^s$. The $\mathbf{E}_{\rm r}^s$ is trivial in the case where $\mathbf{B}_{\rm ext} = \mathrm{B}_0\hat{z}$ is uniform in the cavity space so that $\mathbf{E}_{\rm r}^s = cg_{a\gamma\gamma}a_0B_0\hat{z}$. The homogenous solution with the separation of variables for cylindrical coordinates is $\mathbf{E}_{\rm r}^h = \sum_{m,p} A_h J_m(kr)e^{\pm im\theta}\cos(\frac{p\pi}{L}z)\hat{z}$ where J_m is the mth order of the Bessel function of the first kind, L is the height of the cylinder, and A_h is a coefficient for the electric and magnetic fields.

The boundary condition of the electric field on the perfect conducting surface, $\mathbf{E}_{\rm r}(r = R_0) = 0$, provides a constraint for m and p at the same time as,

$$\sum_{m,p} A_h J_m(kR_0)e^{\pm im\theta}\cos(\frac{p\pi}{L}z) + cg_{a\gamma\gamma}aB_0 = 0. \tag{24}$$

A_h should be a constant for r, θ, z because Eq. (24) must satisfy for every θ, z. Therefore, the only value of m and p that satisfy Eq. (24) for all θ and z is 0. Then, the coefficient A_h can be written as $A_h = -cg_{a\gamma\gamma}aB_0/J_0(kR_0)$. The full expression of the reacted electric and magnetic fields from the axion-photon conversion inside the cavity ($r < R_0$) can be obtained as

$$\mathbf{E}_{\rm cylinder} = cg_{a\gamma\gamma}a\mathrm{B}_0\left(1 - \frac{J_0(kr)}{J_0(kR_0)}\right)\hat{z}, \tag{25a}$$

$$\mathbf{B}_{\rm cylinder} = ig_{a\gamma\gamma}a\mathrm{B}_0\left(\frac{J_1(kr)}{J_0(kR_0)}\right)\hat{\phi}. \tag{25b}$$

Table 1
The resonant modes of cylindrical cavity with radius $R_0 = 9cm$ have been evaluated from analytical solutions. They are also compared with results from the finite element method (FEM). The FEM simulation is based on conductivity $\sigma = 6 \times 10^7 S/m$, and difference between analytic and FEM estimations is defined as $e = 100(\%) \times |A_{\rm Anal} - A_{\rm FEM}|/A_{\rm FEM}$, where A denotes the quantity, such that frequency, Q, and C.

Cavities	Analytical			FEM			Difference(%)		
Modes	Frequency	Q-factor	C-factor	Frequency	Q-factor	C-factor	Frequency	Q-factor	C-factor
TM_{010}	1.278 GHz	49433.04	0.691674	1.275GHz	49447.98	0.691735	0.2868	0.0302	0.0088
TM_{020}	2.935 GHz	74895.03	0.131274	2.927GHz	74913.37	0.131292	0.1053	0.02451	0.0139
TM_{030}	4.601 GHz	93774.20	0.053415	4.588GHz	93795.56	0.053424	0.2828	0.0228	0.0162

When the axion field oscillates with ω_a, the reacted field from the axion-photon interaction stays inside of the resonant cavity. But, if the cavity geometry is matched with the axion mass ($\omega = \omega_a$), the stored fields are enhanced near the geometrical resonant region as $J_0(kR_0) \to 0$. This condition sets $kR_0 = \chi_{0n}$ for the nth zero of J_0.

In the PEC cavity, the energy of the field can be accumulated in the cavity but there would be no power loss due to the PEC condition. It means that the field inside the cavity cannot reach any equilibrium state on the resonant frequency. In the cavity with finite conductivity, however, there exists a certain dissipation of power in the cavity due to the finite conductivity, thereby the field could reach an equilibrium state. It means that the conversion power has a maximum value on the resonant frequency as $J_0(kR_0) \to 0$. In this case, one can set the quality factor Q which is a quantity describing a measure of the power loss in the cavity walls and the sharpness of the response to external excitation. The quality factor Q mainly depends on the conductivity of the cavity wall.

In the case of a resonant cavity with a finite conductivity σ, the cavity behaves like a damped oscillator so that power is dissipated due to the effect of the σ to the field. In this case, the coefficient A_h can be determined from the relationship between the electric field and magnetic field on the cavity surface with finite conductivity as $\mathbf{E}^{\parallel} \simeq \sqrt{\frac{\mu_c \omega}{2\sigma}}(1-i)(\hat{n} \times \frac{\mathbf{B}^{\parallel}}{\mu_c})$, which replaces the PEC boundary condition for the finite conductivity case [30]. This allows us to obtain the expression of A_h for the finite conductivity in a complex form as [31]

$$A_h = -c g_{a\gamma\gamma} a \mathrm{B}_0 \times \frac{1}{\alpha} = -\frac{c g_{a\gamma\gamma} a \mathrm{B}_0}{\left(J_0(kR_0) - \sqrt{\frac{\mu_0 \omega}{2\sigma}} \frac{1+i}{c\mu_0} J_1(kR_0)\right)}, \tag{26}$$

The field solution in a resonant cavity with a finite conductivity is, therefore, obtained as follows

$$\mathbf{E}^{\sigma}_{\rm cylinder} = c g_{a\gamma\gamma} a \mathrm{B}_0 \left(1 - I(\omega) \frac{J_0(kr)}{e^{i\mathrm{Arg}[\alpha]}}\right) \hat{z}, \tag{27a}$$

$$\mathbf{B}^{\sigma}_{\rm cylinder} = i g_{a\gamma\gamma} a \mathrm{B}_0 \left(I(\omega) \frac{J_1(kr)}{e^{i\mathrm{Arg}[\alpha]}}\right) \hat{\phi}. \tag{27b}$$

In Eq. (27), one can define the enhancement factor $I(\omega)$ as a function of the quality factor Q near $\omega \simeq \omega_0$ as the following

$$\begin{aligned} I(\omega) = \frac{1}{|\alpha|} &= \left| \frac{1}{\left(J_0(kR_0) - \sqrt{\frac{\mu_0 \omega}{2\sigma}} \frac{1+i}{c\mu_0} J_1(kR_0)\right)} \right| \\ &\approx \sqrt{\frac{2\sigma\mu_0 c^2}{\omega_0}} \left| \frac{1}{J_1\left(\omega_0 \frac{R_0}{c}\right)} \right| \\ &\quad \times \frac{1}{\sqrt{1 + 4\left(\sigma\omega_0\mu_0 R_0^2/2\right)\left(\frac{\omega}{\omega_0} - 1\right)^2}} \\ &\equiv \frac{A}{\sqrt{1 + 4Q^2\left(\frac{\omega}{\omega_0} - 1\right)^2}}, \end{aligned} \tag{28}$$

where $A = \sqrt{\frac{2\sigma\mu_0 c^2}{\omega_0}} \left| \frac{1}{J_1\left(\omega_0 \frac{R_0}{c}\right)} \right|$. The quality factor Q becomes $Q \approx \sqrt{\sigma\omega_0\mu_0 R_0^2/2} = \frac{R_0}{\delta_0}$ with skin depth δ_0.

Table 1 shows the resonant frequencies of TM_{0n0} ($n = 1, 2, 3$) modes in the cylindrical cavity evaluated using analytical field estimation, and compared with the eigenmode frequency evaluated from the finite element method (FEM). The frequencies, quality factor(Q), and form factor(C) obtained from the analytical estimates are very close to those from FEM.

3.2. Resonance regime in a toroidal cavity with a circular cross section

The toroidal cavity has been considered as a very attractive geometry for axion haloscope searches because the conversion power would be improved by having the rather large volume from the toroidal geometry. Recently, there was a proposed experiment looking for an axion with a prototype toroidal resonant cavity called ACTION at CAPP [17].

We consider a toroidal cavity having a geometry with the major radius R and minor radius r_0 as a resonant cavity. The simple toroidal coordinate is (r, ϑ, φ) where ϑ is the counterclockwise angle in the vertical section of the toroid, and φ is the azimuthal angle as shown in Fig. 2. The transformation to the ordinary Cartesian coordinate will be

$$\begin{aligned} x &= (R + r\cos\vartheta)\cos\varphi, \\ y &= (R + r\cos\vartheta)\sin\varphi, \\ z &= r\sin\vartheta. \end{aligned}$$

For the toroidal cavity, the external magnetic field, $\mathbf{B}_{\rm ext}$, is applied along the $\hat{\varphi}$ direction as

$$\mathbf{B}_{\rm ext} = \frac{\mathrm{B}_0}{R + r\cos\vartheta} \hat{\varphi},$$

which still satisfies the condition for the haloscope searches, $\nabla \times \mathbf{B}_{\rm ext} = 0$, in the toroidal coordinate.

Since the differential equation in Eq. (23) is not separable in the toroidal coordinate, we applied a trial solution in approximate form. The inseparable solution W for wave equation has a dependence of r, and ϑ as $W = \sum_n W_n(r, \vartheta)$. The differential equation that the $W(r, \vartheta)$ must satisfy is

$$\begin{aligned} \Bigg[&\frac{\partial^2}{\partial r^2} + \frac{\partial^2}{r^2 \partial\vartheta^2} + \left(\frac{1}{r} + \frac{\cos\vartheta}{R + r\cos\vartheta}\right)\frac{\partial}{\partial r} \\ &- \frac{\sin\vartheta}{r(R + r\cos\vartheta)}\frac{\partial}{\partial\vartheta} + k^2 \Bigg] W(r, \vartheta) = 0. \end{aligned} \tag{29}$$

Table 2
The resonant frequencies of TM_{0n0} $(n = 1, 2, 3)$ like modes in the toroidal cavity with minor radius $r_0 = 9cm$ and major radius $R = 90cm$ evaluated from analytical solutions, and compared with results from the finite element method (FEM). The simulation is based on conductivity $\sigma = 6 \times 10^7 S/m$, and difference between analytic and FEM estimations is defined as $e = 100(\%) \times |A_{\text{Anal}} - A_{\text{FEM}}|/A_{\text{FEM}}$, where A denotes the quantity, such that frequency, Q, and C.

Cavities	Analytical			FEM			Difference(%)		
Modes	Frequency	Q-factor	C-factor	Frequency	Q-factor	C-factor	Frequency	Q-factor	C-factor
TM_{010}	1.278 GHz	49243.44	0.691322	1.2757GHz	49528.6236	0.6908	0.2217	0.5758	0.0756
TM_{020}	2.935 GHz	74528.75	0.131884	2.9270GHz	74936.6285	0.1314	0.1177	0.5443	0.3745
TM_{030}	4.601 GHz	93306.70	0.053702	4.588GHz	93807.5769	0.0535	0.27778	0.5339	0.4158

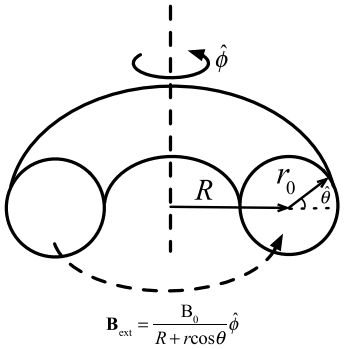

Fig. 2. Toroidal cavity with circular cross section. The major radius is R and the minor radius is r_0. The static magnetic field $\mathbf{B}_{\text{ext}}$ has been applied inside the torus along the $\hat{\varphi}$ direction as $\mathbf{B}_{\text{ext}} = \frac{\mathrm{B}_0}{R + r\cos\vartheta}\hat{\varphi}$.

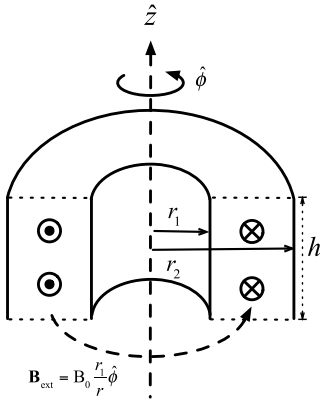

Fig. 3. Toroidal cavity made with two infinite concentric cylinders with inner radius r_1 and outer radius r_2. The static magnetic field $\mathbf{B}_{\text{ext}}$ has been applied only between two cylinders along the $\hat{\phi}$ direction as $\mathbf{B}_{\text{ext}} = \mathrm{B}_0\frac{r_1}{r}\hat{\phi}$.

The trial function is $W_n(r, \vartheta) = f_n(r)/(R + r\cos\vartheta)^n$, to eliminate the coordinate mixing term $R + r\cos\vartheta$. Using this notation, the homogeneous solution for the electric field becomes $E^h_{\text{toroid}}(r, \vartheta) = \sum_n A^{\text{tor}}_n W_n(r, \vartheta)$, where A^{tor}_n is a coefficient defined from the boundary condition.

In the ideal case of PEC, a set of solutions for the electric and magnetic fields can be acquired from the lowest order of the inseparable solution $W_n(r, \vartheta)$ as $W_1(r, \vartheta) \approx \frac{f_1(r)}{R + r\cos\vartheta}$. By putting this trial solution into Eq. (29), we can get a differential equation for $f_1(r)$. If we ignore the higher order of $1/(R + r\cos\vartheta)^2$ term, $f_1(r)$ can be expressed with $J_0(kr)$. As a result, the electromagnetic field in the lowest order can be given as

$$\mathbf{E}_{\text{toroid}} = cg_{a\gamma\gamma}a\left(\frac{\mathrm{B}_0}{R + r\cos\vartheta}\right)\left(1 - \frac{J_0(kr)}{J_0(kr_0)}\right)\hat{\varphi}, \tag{30a}$$

$$\mathbf{B}_{\text{toroid}} = ig_{a\gamma\gamma}a\left(\frac{\mathrm{B}_0}{R + r\cos\vartheta}\right)\left(\frac{J_1(kr)}{J_0(kr_0)}\right)\hat{\vartheta}. \tag{30b}$$

Like the cylindrical case, the stored fields can be enhanced as $J_0(kr_0) \to 0$ so that $kr_0 = \chi_{0l}$ can be lth zero of J_0. The approximated solution for the electromagnetic field is almost identical to the one for the cylindrical case. But, because of the approximation we took for the trial solution of the wave equation in Eq. (29), this set of solutions for electric and magnetic fields in Eq. (30) has a certain limitation in terms of accuracy. Especially when the inverse aspect ratio $(\eta = r_0/R)$ is larger than 0.5, solutions from this approximation become inappropriate. However, since it is not realistic to have a toroidal cavity with an inverse aspect ratio larger than 0.5, this approximation is still valid for practical purposes.

In the case of a resonant cavity with a finite conductivity σ, the electromagnetic field has the enhancement factor $I(\omega)$ which was defined in Eq. (26).

$$\mathbf{E}^{\sigma}_{\text{toroid}} = cg_{a\gamma\gamma}a\left(\frac{\mathrm{B}_0}{R + r\cos\vartheta}\right)\left(1 - I(\omega)\frac{J_0(kr)}{e^{i\mathrm{Arg}[\alpha]}}\right)\hat{\varphi}, \tag{31a}$$

$$\mathbf{B}^{\sigma}_{\text{toroid}} = ig_{a\gamma\gamma}a\left(\frac{\mathrm{B}_0}{R + r\cos\vartheta}\right)\left(I(\omega)\frac{J_1(kr)}{e^{i\mathrm{Arg}[\alpha]}}\right)\hat{\vartheta}, \tag{31b}$$

Table 2 shows the resonant frequencies of TM_{0n0} $(n = 1, 2, 3)$ like modes in the toroidal cavity evaluated using analytical field estimation, and compared with the eigenmode frequency evaluated from the finite element method (FEM). The frequencies, quality factor(Q), and electric form factor(C) obtained from the analytical estimates are very close to the those from FEM.

3.3. Resonance regime with two infinite concentric cylinders

Recently, an experimental idea searching for axions with a toroidal magnetic field with a square cross-section has been developed [22,32]. We applied the Maxwell's equations in the case of a toroid made with two concentric cylinders to evaluate electromagnetic field. We assumed that the toroidal cavity is made with two concentric cylindrical cavities with inner radius r_1, outer radius r_2 as shown in Fig. 3. We also assumed that the height of the cavity to be $h \to \infty$ and the thickness of the cavity to be $\delta \to 0$ for simplicity in our estimation of the fields. The external magnetic field is assumed to be applied only between two cavities, r_1 and r_2 as $\mathbf{B}_{\text{ext}} = \mathrm{B}_0\frac{r_1}{r}\hat{\phi}$ $(r_1 \le r \le r_2)$ and $\mathbf{B}_{\text{ext}} = 0$ elsewhere. From the wave equations for $\mathbf{E}_{\text{r}}$ and $\mathbf{B}_{\text{r}}$ in a cylindrical coordinate from Eq. (25), we can estimate the reacted field in the region between two concentric cavities as

$$\begin{aligned}\mathbf{E}_{\text{rect}} = \mathbf{E}^s_{\text{rect}} + \mathbf{E}^h_{\text{rect}} &= cg_{a\gamma\gamma}a\mathrm{B}_0\frac{r_1}{r}\hat{\phi} \\ &+ \left[AJ_1\left(\sqrt{k^2 - n^2}r\right) + BY_1\left(\sqrt{k^2 - n^2}r\right)\right] \\ &\times \left(Ce^{inz} + De^{-inz}\right)\hat{\phi},\end{aligned} \tag{32a}$$

$$\begin{aligned}\mathbf{B}_{\text{rect}} = &\frac{\sqrt{k^2 - n^2}}{i\omega}\left[AJ_0\left(\sqrt{k^2 - n^2}r\right) + BY_0\left(\sqrt{k^2 - n^2}r\right)\right] \\ &\times \left(Ce^{inz} + De^{-inz}\right)\hat{z} \\ &- \frac{n}{\omega}\left[AJ_1\left(\sqrt{k^2 - n^2}r\right) + BY_1\left(\sqrt{k^2 - n^2}r\right)\right]\end{aligned}$$

Table 3
The resonant frequencies of TM_{0n0} ($n = 1, 2, 3$) like modes in the toroidal cavity made with two infinite concentric cylinders ($r_1 = 85\ cm,\ r_2 = 170cm$). These frequencies have been evaluated from analytical solutions and compared with results from the finite element method (FEM)

Cavities	Two infinite concentric cylinders	
Modes	Analytical	FEM
TM_{010}	305.25 MHz	305.04 MHz
TM_{020}	602.79 MHz	602.38 MHz
TM_{030}	901.88 MHz	901.26 MHz

$$\times \left(Ce^{inz} - De^{-inz}\right)\hat{r}. \tag{32b}$$

The coefficients for the $\mathbf{B}_{\text{rect}}$ can be related to those from the $\mathbf{E}_{\text{rect}}$ through Eq. (21d). From the symmetry condition, $\lim_{z\to\infty}(C - D)\sin(nz) = 0$, Eq. (32) can be simplified with $n = 0$ as

$$\mathbf{E}_{\text{rect}} = \left(cg_{a\gamma\gamma}aB_0\frac{r_1}{r} + AJ_1(kr) + BY_1(kr)\right)\hat{\phi}, \tag{33a}$$

$$\mathbf{B}_{\text{rect}} = -\frac{i}{c}\left(AJ_0(kr) + BY_0(kr)\right)\hat{z}. \tag{33b}$$

If we use the PEC as the boundary condition at both ends of the cavity surfaces, r_1 and r_2, one can use $\mathbf{E}_{\text{rect}}(r_1) = \mathbf{E}_{\text{rect}}(r_2) = 0$ to determine the unknown coefficients, A and B as

$$A = -cg_{a\gamma\gamma}aB_0\left(\frac{1}{r_2}\right)\left(\frac{Y_1(kr_2)r_2 - Y_1(kr_1)r_1}{J_1(kr_1)Y_1(kr_2) - J_1(kr_2)Y_1(kr_1)}\right), \tag{34a}$$

$$B = -cg_{a\gamma\gamma}aB_0\left(\frac{1}{r_2}\right)\left(\frac{-J_1(kr_2)r_2 + J_1(kr_1)r_1}{J_1(kr_1)Y_1(kr_2) - J_1(kr_2)Y_1(kr_1)}\right), \tag{34b}$$

where J_n and Y_n is the nth order of the first and second kind of Bessel function, respectively. As shown in the previous section, one could estimate the solution for the finite conductivity case with a continuity boundary condition.

Table 3 shows the resonant frequencies of TM_{0n0} ($n = 1, 2, 3$) like modes evaluated using analytical field estimation comparing with the eigenmode frequency evaluated from the finite element method.

3.4. Long wavelength regime

Most experiments that utilize a resonant cavity under an homogeneous magnetic field are designed to detect microwave photons generated from the axion-photon conversion. The size of the magnetic field mainly depends on the target axion mass they look for. But, these axion haloscope experiments with resonant cavities have a very narrow band of search range in the microwave regime.

Recently, LC circuits or the other broadband searches that can be used with an external magnetic field have been suggested to search for axions with a mass range in $m_a \ll 10^{-6}$ eV [21,22]. If the axion mass is very light, the Compton wavelength of the axion becomes much longer than the typical size of the cavity in current experiments ($\lambda_a \gg R_0$). In this regime, the reacted electromagnetic fields would not resonate in the cavity mode any more. The electromagnetic field rather slowly oscillates with a frequency corresponding to the axion mass. Therefore, they can be treated in the frame of a quasi-static approximation. But, the behavior of the field still can be approximately estimated from the solutions obtained from the resonance regime by taking $kR_0 \ll 1$ limit.

Unlike the resonant regime in the cavity, the enhancement from the quality factor Q of the cavity cannot be expected in the long wavelength regime because the field would not resonate. It implies that the energy of the field cannot be stored inside the cavity but is rather dissipated out of the cavity. However, as a return, a wide frequency range can be searched in the long wavelength regime because there is no bandwidth limit in off-resonant frequency region.

For an electromagnetic field in a cylindrical cavity, this can be approximately expressed from Eq. (25) by taking $kR_0 \ll 1$ limit as

$$\mathbf{E}_{\text{r}} \approx cg_{a\gamma\gamma}aB_0\left(\left(\frac{kr}{2}\right)^2 - \left(\frac{kR_0}{2}\right)^2\right)\hat{z},\ (r < R_0) \tag{35a}$$

$$\mathbf{B}_{\text{r}} \approx ig_{a\gamma\gamma}a_0B_0e^{-i\omega_a t}\frac{kr}{2}\hat{\phi} = -\frac{g_{a\gamma\gamma}}{2c}rB_0\dot{a}\hat{\phi}\ (r < R_0). \tag{35b}$$

As seen in Eq. (35a), the electric field has a maximum strength at the center ($r = 0$), but approaches to zero as it comes closer to the cavity surface ($r = R_0$). The electric field at the center shows similar behavior with the one in McAllister et al. [19] shown in Eq. (6a). There is also $(kR_0)^2$ difference between them. However, the biggest difference is the field near the cavity surface ($r = R_0$). Although Eq. (6a) shows no r dependence, the electric field in Eq. (35a) clearly shows that it becomes zero at the cavity surface. Moreover, the electromagnetic fields in Eq. (35) are compatible solutions, thereby fully satisfying the Maxwell-Faraday relationship in Eq. (9) unlike one in McAllister et al. [19].

While the electric field is suppressed by an order of $(kr)^2$ in this long wavelength regime, the magnetic field in Eq. (35) is still in the first order of kr. Therefore, it should be possible to search for axions in the long wavelength regime by detecting the magnetic field with a sensitive magnetometer coupled with an LC circuit [21]. The solution of the magnetic field with field continuity boundary condition gives the exactly same result as the one in the PEC condition in the leading order of kr.

ABRACADABRA is a new experiment to search for axion dark matter over a broad range of axion masses, particularly $m_a \ll 10^{-6}$ eV [22,32]. This experiment is designed to search for the axion-induced field, $\mathbf{B}_a$, generated from a toroidal magnetic field through a superconducting pickup loop in the center of a toroidal magnet. As mentioned before, they estimated the magnetic field in the quasi-magnetostatic condition, where the oscillating current $\mathbf{J}_a$ directly induces the magnetic field. We show that the magnetic field in the center of the toroidal magnet can be derived from the solution of the magnetic field in Eq. (33) by taking the $kr_1 \ll 1$ and $kr_2 \ll 1$ limit with the field continuity boundary condition. We set the thickness of the concentric cylinders to zero and make fields be continuous at the boundary. For a toroidally applied external magnetic field, $\mathbf{B}_{\text{ext}} = B_0\frac{r_1}{r}\hat{\phi}$, between two concentric cylindrical surface currents, the solutions for all of space can be written as follows by following from the argument leading to Eq. (33)

$$\mathbf{E}_{\text{r}} = \begin{cases} A_{in}J_1(kr)\hat{\phi} & r < r_1 \\ \left(AJ_1(kr) + BY_1(kr) + cg_{a\gamma\gamma}aB_0\frac{r_1}{r}\right)\hat{\phi} & r_1 < r < r_2 \\ A_{out}H_1^+(kr)\hat{\phi} & r > r_2 \end{cases} \tag{36a}$$

$$\mathbf{B}_{\text{r}} = \begin{cases} A_{in}J_0(kr)\hat{z} & r < r_1 \\ \left(AJ_0(kr) + BY_0(kr)\right)\hat{z} & r_1 < r < r_2 \\ A_{out}H_0^+(kr)\hat{z} & r > r_2. \end{cases} \tag{36b}$$

The simultaneous equations for coefficients, A_{in}, A, B, A_{out}, become

$$\begin{aligned} &A_{in}J_1(kr_1) = cg_{a\gamma\gamma}aB_0 + AJ_1(kr_1) + BY_1(kr_1), \\ &A_{in}J_0(kr_1) = AJ_0(kr_1) + BY_0(kr_1), \\ &cg_{a\gamma\gamma}a\frac{B_0r_1}{r_2} + AJ_1(kr_2) + BY_1(kr_2) = A_{out}H_1^+(kr_2), \\ &AJ_0(kr_2) + BY_0(kr_2) = A_{out}H_0^+(kr_2). \end{aligned} \tag{37}$$

In the $kr_{1,\,2} \ll 1$ limit, we can get $A = -cg_{a\gamma\gamma}aB_0kr_1\left(\gamma + \ln\left(\frac{kr_2}{2}\right)\right)$, $B = \frac{1}{2}\pi kcg_{a\gamma\gamma}aB_0r_1$, respectively. A detail of our

approximation is presented in the Appendix. The corresponding magnetic field in this region becomes,

$$\mathbf{B}_{\mathrm{r}} = \frac{g_{a\gamma\gamma}\dot{a}\mathrm{B}_0}{c} r_1 \left(\ln\left(\frac{kr}{2}\right) + \gamma \right) \hat{z}, \ (r_1 < r < r_2). \tag{38}$$

The magnetic field in the central region of the toroidal cavity made with two concentric cylinders becomes

$$\mathbf{B}_{\mathrm{r}} = i g_{a\gamma\gamma} a \mathrm{B}_0 k r_1 \ln\left(\frac{r_2}{r_1}\right)\hat{z} = -\frac{g_{a\gamma\gamma}\dot{a}\mathrm{B}_0 r_1}{c} \ln\left(\frac{r_2}{r_1}\right)\hat{z}, \ (0 \le r < r_1). \tag{39}$$

4. Electromagnetic energy and power in cavity modes

In the haloscope search for axions with a resonant cavity, the axion-photon conversion is detected through the signal power of the resonant frequency which corresponds to the axion mass. In the equilibrium state, the power loss (P_{loss}) through the microwave cavity wall is assumed to be equivalent with the axion to photon conversion power inside the cavity P_{conv} as,

$$P_{\mathrm{conv}} = P_{\mathrm{loss}} = \frac{\omega U_{\mathrm{tot}}}{Q} = \frac{\omega\,(U_{\mathrm{E}} + U_{\mathrm{B}})}{Q}, \tag{40}$$

where U_{tot} is the total stored energy in the electric and magnetic field inside the cavity as $U_{\mathrm{tot}} = U_{\mathrm{E}} + U_{\mathrm{B}}$. The quality factor Q depends on the material properties of the cavity walls as shown in previous section.

On the resonance frequency of the cavity modes, the conversion power P can be expressed in terms of a cavity form factor C as

$$P_{mnp} = g_{a\gamma\gamma}^2 \frac{\rho_a}{m_a} \int dV |B_{\mathrm{ext}}|^2 C_{mnp} \min(Q_0, Q_a), \tag{41}$$

where m, n, p are the indices of the resonant mode. The parameters are given by B_{ext}, the external magnetic field strength, V, the volume of the cavity, Q_0, the unloaded quality factor of the cavity, and Q_a, the quality factor of axions. The signal power is linearly dependent on the C_{mnp}. Therefore, the mode of interest have the highest possible C_{mnp}, given by

$$C_{mnp} = \frac{\left|\int \mathbf{E_{mnp}} \cdot \mathbf{B}_{\mathrm{ext}} dV\right|^2}{\int |\mathbf{B}_{\mathrm{ext}}|^2 dV \int \epsilon_r \left|\mathbf{E_{mnp}}\right|^2 dV}, \tag{42}$$

where $\mathbf{E_{mnp}}$ is the electric field of the mode, ϵ_r is the permittivity within the cavity. Eq. (41) shows that the sensitivity of a haloscope search strongly depends on the static magnetic field and the direction of the resonant electric field. For the transverse magnetic field (TM_{0n0}) considered in haloscope searches with cylindrical resonant cavities, the form factor can be expressed as $C_{0n0} = \frac{4}{\chi_{0n}^2}$. The lowest mode, TM_{010} is mainly interested in the haloscope search with cavities due to the higher form factor value as $C_{010} \approx 0.69$.

However, Eq. (41) is valid only the resonance frequency. If the conversion takes place beyond the bandwidth of the resonance, it would be unsuitable to estimate the conversion power directly from Eq. (41). The generalized expression of the conversion power, therefore, would be necessary if the off-resonance region is considered for the axion searches as well. The generalized expression of the conversion power for any frequency can be obtained from the following relations getting from Maxwell's equations in Eq. (22) as

$$\frac{\partial u_{\mathrm{tot}}}{\partial t} + \nabla \cdot \mathbf{S} = \left(i\omega_a \sqrt{\frac{\epsilon_0}{\mu_0}} g_{a\gamma\gamma} a_0 B_0 e^{-i\omega_a t} \right) \cdot \mathbf{E}_{\mathrm{r}}, \tag{43a}$$

$$\oint \mathbf{S} \cdot \hat{n} dA + 2i\omega\delta U = -\frac{1}{2} \int \left(i\omega_a \sqrt{\frac{\epsilon_0}{\mu_0}} g_{a\gamma\gamma} a_0 B_0 e^{-i\omega_a t} \right) \cdot \mathbf{E}_{\mathrm{r}} dV, \tag{43b}$$

where $u_{\mathrm{tot}} = u_{\mathrm{E}} + u_{\mathrm{B}}$ is total energy density, $\mathbf{S} = \frac{1}{2}\left(\mathbf{E}_{\mathrm{r}} \times \mathbf{B}_{\mathrm{r}}^*\right)$ is Poynting vector with phasor expression, and $\delta U = U_{\mathrm{E}} - U_{\mathrm{B}}$ is the energy difference.

By comparing Eq. (43a) with a differential form of the Poynting theorem, we can get the axion induces current as

$$\mathbf{J}_a = -\sqrt{\frac{\epsilon_0}{\mu_0}} g_{a\gamma\gamma} \dot{a} \mathbf{B}_{\mathrm{ext}}. \tag{44}$$

In addition, Eq. (43b) can be divided into real and imaginary parts as

$$\mathrm{Re}\left[\oint \mathbf{S} \cdot \hat{n} dA\right] = -\frac{1}{2}\mathrm{Re}\left[\int \mathbf{J}_a^* \cdot \mathbf{E}_{\mathrm{r}} dV\right], \tag{45a}$$

$$\mathrm{Im}\left[\oint \mathbf{S} \cdot \hat{n} dA\right] + 2\omega\delta U = -\frac{1}{2}\mathrm{Im}\left[\int \mathbf{J}_a^* \cdot \mathbf{E}_{\mathrm{r}} dV\right]. \tag{45b}$$

If we take the boundary including the conducting surface in Eq. (45b), the imaginary part of Poynting vector $\mathbf{S}$ becomes zero as $\mathrm{Im}\left[\oint \mathbf{S} \cdot \hat{n} dA\right] = 0$ at the boundary. Therefore, the δU becomes

$$\delta U = -\frac{1}{4\omega}\mathrm{Im}\left[\int \mathbf{J}_a^* \cdot \mathbf{E}_{\mathrm{r}} dV\right]. \tag{46}$$

In the case of a resonant cavity with a finite conductivity σ, the Joule heating, $\mathbf{J}_e = \sigma \mathbf{E}_{\mathrm{r}}$, has to be considered as well in Eq. (45a) due to the finite conductivity of the cavity as,

$$\mathrm{Re}\left[\oint \mathbf{S} \cdot \hat{n} dA\right] = -\frac{1}{2}\mathrm{Re}\left[\int \mathbf{J}_a^* \cdot \mathbf{E}_{\mathrm{r}} dV\right] - \frac{1}{2}\int \sigma\, |\mathbf{E}_{\mathrm{r}}|^2\, dV \tag{47a}$$

$$\frac{1}{2}\mathrm{Im}\left[\int \mathbf{J}_a^* \cdot \mathbf{E}_{\mathrm{r}} dV\right] = -2\omega\delta U - \mathrm{Im}\left[\oint \mathbf{S} \cdot \hat{n} dA\right], \tag{47b}$$

The imaginary part of the equation remains the same as Eq. (45b), and the Poynting vector in Eq. (47) can still be suppressed by taking a boundary containing the cavity. Now $\mathbf{J}_a^* \cdot \mathbf{E}_{\mathrm{r}}$ is complex because the $\mathbf{E}_{\mathrm{r}}$ is complex with finite conductivity as shown in Eq. (26). If we assume that the Joule heating is totally coming from the loss of axion power via axion photon conversion, the conversion power can be expressed with the loss power through Joule heating as $P_{\mathrm{conv}} = \frac{1}{2}\mathrm{Re}\left[\int \mathbf{J}_a^* \cdot \mathbf{E}_{\mathrm{r}} dV\right]$ from Eq. (47). Then, the complex value T can be defined from the real and imaginary parts in Eq. (47) as,

$$T = -\frac{1}{2}\int \mathbf{J}_a^* \cdot \mathbf{E}_{\mathrm{r}} dV = P_{\mathrm{conv}} + 2i\omega\delta U, \tag{48}$$

where the real part of T is the Joule heating power that we detect via the cavity and the imaginary part of T is the energy difference δU. Applying the complex conjugate T^* to get the absolute value of T gives an expression of T as,

$$|T|^2 = \frac{1}{4}\frac{\epsilon_0}{\mu_0}(g_{a\gamma\gamma}\omega a_0)^2 \int |B_0 \cdot \epsilon_r E|^2\, dV = P_{\mathrm{conv}}^2 + 4\omega^2\delta U^2. \tag{49}$$

From Eq. (49), the conversion power P_{conv} can be expressed as

$$P_{\mathrm{conv}} = \sqrt{|T|^2 - 4\omega^2\delta U^2} \tag{50}$$

By dividing Eq. (49) into P_{conv}, one can get following expression of the conversion power as,

$$P_{\mathrm{conv}} = \frac{1}{2\mu_0}\omega(g_{a\gamma\gamma}a_0)^2 \int |B_{\mathrm{ext}}|^2 dV Q C_{form} \frac{2U_{\mathrm{E}}}{U_{\mathrm{tot}}} - 4\omega Q \frac{\delta U^2}{U_{\mathrm{tot}}}, \tag{51}$$

where $Q = \omega U/P$ is the quality factor. The generalized form factor, C_{form}, for any frequency is defined as

$$C_{form} \equiv \frac{\left|\int \mathbf{E_r} \cdot \mathbf{B}_{\mathrm{ext}} dV\right|^2}{\int |\mathbf{B}_{\mathrm{ext}}|^2 dV \int \epsilon_r \left|\mathbf{E_r}\right|^2 dV}. \tag{52}$$

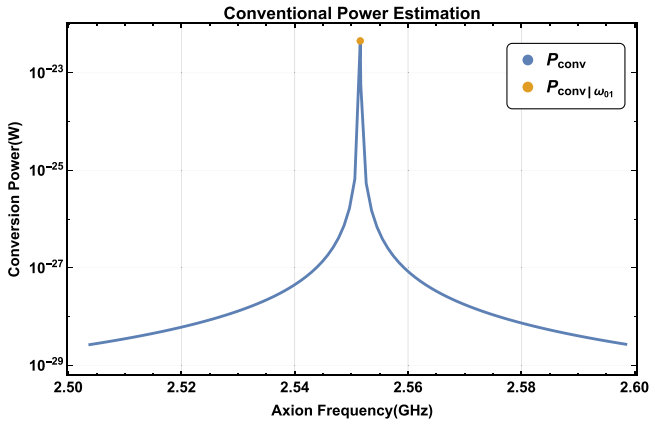

Fig. 4. The conversion power estimated from Eq. (51) compared with Eq. (53) near TM_{010} mode. The overall behavior of the conversion power in off resonance region shows Cauchy-Lorentz distribution. The parameters to estimate the plot are following; (1) KSVZ axion model parameter $g_{a\gamma\gamma}f_a = -2.3 \times 10^{-3}$, (2) initial misalignment angle $a_0/f_a = 3.7 \times 10^{-19}$ [18], (3) 8Tesla of the external magnetic field, (4) $6 \times 10^7 S/m$ of the cavity conductivity, (5) 45mm of the cavity radius, and (6) 1m height of the cavity.

Eq. (51) expresses the conversion power in any frequency range including on-resonance ones. As the frequency ω_a approaches to the resonant one ω_{0n} in the cavity as $\omega_a \to \omega_{0n}$, the form factor goes to the resonant field form factor in Eq. (42) ($C_{form} \to C_{0n}$), and $U_E \approx U_B$ so that we can apply $\frac{2U_E}{U_{tot}} \to 1$, and $\delta U \to 0$. Therefore, only first term contributes to the conversion power. The conversion power on the resonance frequency ω_{0n} now becomes,

$$P_{conv}|_{\omega_{0n}} = \frac{1}{2\mu_0}\omega_{0n}(g_{a\gamma\gamma}a_0)^2 \int |B_{ext}|^2 dV Q C_{0n}, \tag{53}$$

which is the conversion power on the resonance frequency used in the haloscope searches [16].

The first term in Eq. (51) remains almost unchanged even in off-resonance region. But, the second term becomes larger as the frequency is tuned away from the on-resonance frequency because δU cannot be negligible in the off-resonance region anymore. As a result, the total conversion power is reduced quickly in off-resonance region as shown in Fig. 4. It implies that the energy difference has to be taken into account in the estimation of the conversion power if the off-resonance region is in the interest of axion searches. The overall behavior of the conversion power follows the Cauchy-Lorentz distribution.

5. Conclusion

We applied an effective approximation to Maxwell's equations to get a decoupled Maxwell's equations only for the reacted electromagnetic fields from axion-photon interaction. We solved the decoupled Maxwell's equations rigorously under various geometrical conditions in the axion resonance regime (10^{-6} eV $< m_a <$ 10^{-4} eV) to obtain the solution of the electromagnetic fields. In the long wavelength regime ($m_a \ll 10^{-6}$ eV), the electromagnetic fields were derived directly from the solutions in the resonance regime by taking the long wavelength limit. Axion-photon conversion power was examined from the Maxwell's equations in the axion resonance regime. On the resonant frequency, the energy difference between the electric and magnetic fields is almost negligible, but it would be considerably larger when the frequency move into off-resonant region. Therefore, this difference may have to be taken into consideration if the off-resonant region is also of interest for axion haloscope searches with a cavity.

Acknowledgment

This work was supported by Institute for Basic Science under Grant No. IBS-R017-D1-2019-a00.

Appendix. Solution for concentric cylinders in continuous boundary condition

The solutions of the A, B without any approximation are,

$$\begin{aligned} A &= -\frac{i}{2}\pi c g_{a\gamma\gamma} a\pi kr_1 (J_0(kr_1) - H_0^+(kr_2)) \\ B &= \frac{1}{2}\pi c g_{a\gamma\gamma} a\pi kr_1 J_0(kr_1). \end{aligned} \tag{A.1}$$

The Hankel function H_0^+ can be written as $H_0^+ = J_0 + iY_0$. If we approximate $kr_{1,2} \ll 1$, then the asymptotic behavior of the Bessel functions are,

$$\begin{aligned} J_0(kr) &\simeq 1, \\ Y_0(kr) &\simeq \frac{2}{\pi}\left(\ln\left(\frac{kr}{2}\right) + \gamma\right). \end{aligned} \tag{A.2}$$

Then we could get A, B in Eq. (37).

References

[1] R.D. Peccei, H.R. Quinn, Phys. Rev. Lett. 38 (1977) 1440.
[2] D.J.E. Marsh, Phys. Rep. 643 (2016) 1, arXiv:1510.07633.
[3] J. Preskill, M.B. Wise, F. Wilczek, Phys. Lett. B 120 (1983) 127.
[4] J.E. Kim, Phys. Rev. Lett. 43 (1979) 103.
[5] M.A. Shifman, A.I. Vainshtein, V.I. Zakharov, Nuclear Phys. B 166 (1980) 493.
[6] M. Dine, W. Fischler, M. Srednicki, Phys. Lett. B 104 (1981) 199.
[7] A.R. Zhitnitsky, Sov. J. Nucl. Phys. 31 (1980) 260, (Yad. Fiz. 31 (1980) 497).
[8] M. Srednicki, Nuclear Phys. B 260 (1985) 689.
[9] H. Primakoff, Phys. Rev. 81 (1951) 899.
[10] P. Sikivie, Phys. Rev. Lett. 51 (1983) 1415.
[11] K. van Bibber, N.R. Dagdeviren, S.E. Koonin, A.K. Kerman, H.N. Nelson, Phys. Rev. Lett. 59 (1987) 759.
[12] F. Wilczek, Phys. Rev. Lett. 58 (1987) 1799.
[13] L. Visinelli, Modern Phys. Lett. A 28 (2013) 1350162.
[14] S.C. Tiwari, Modern Phys. Lett. A 30 (2015) 1550204-306.
[15] A.G. Dias, A.C.B. Machado, C.C. Nishi, A. Ringwald, P. Vaudrevange, J. High Energy Phys. 6 (2014) 37, arXiv:1403.5760 [hep-ph].
[16] P. Sikivie, Phys. Rev. D 32 (1985) 2988.
[17] J. Choi, H. Themann, M.J. Lee, B.R. Ko, Y.K. Semertzidis, Phys. Rev. D 96 (2017) 061102, arXiv:1704.07957 [hep-ex].
[18] M.S. Turner, Phys. Rev. D 33 (1986) 889.
[19] B.T. McAllister, S.R. Parker, M.E. Tobar, Phys. Rev. Lett. 116 (2016) 161804, arXiv:1512.05547 [hep-ph].
[20] B.T. McAllister, M. Goryachev, J. Bourhill, E.N. Ivanov, M.E. Tobar, ArXiv e-prints, 2018, arXiv:1803.07755 [physics.ins-det].
[21] P. Sikivie, N. Sullivan, D.B. Tanner, Phys. Rev. Lett. 112 (2014) 131301, arXiv:1310.8545 [hep-ph].
[22] J.L. Ouellet, C.P. Salemi, J.W. Foster, R. Henning, Z. Bogorad, J.M. Conrad, J.A. Formaggio, Y. Kahn, J. Minervini, A. Radovinsky, N.L. Rodd, B.R. Safdi, J. Thaler, D. Winklehner, L. Winslow, ArXiv e-prints, 2018, arXiv:1810.12257 [hep-ex].
[23] B.R. Ko, H. Themann, W. Jang, J. Choi, D. Kim, M.J. Lee, J. Lee, E. Won, Y.K. Semertzidis, Phys. Rev. D 94 (2016) 111702, arXiv:1608.00843 [hep-ph].
[24] Y. Kim, D.O. Kim, J. Jeong, Y.C. Shin, Y. Semertzidis, APS Meeting Abstracts, 2018, pp. Y09.006.
[25] Y. Kim, D.O. Kim, J. Jeong, Y.C. Shin, Y. Semertzidis, 14th Patras Workshop on Axions, WIMPs and WISPs, 2018.
[26] S.J. Asztalos, G. Carosi, C. Hagmann, D. Kinion, K. van Bibber, M. Hotz, L.J. Rosenberg, G. Rybka, J. Hoskins, J. Hwang, P. Sikivie, D.B. Tanner, R. Bradley, J. Clarke, ADMX Collaboration, Phys. Rev. Lett. 104 (2010) 041301, arXiv:0910.5914 [astro-ph.CO].
[27] M.S. Safronova, D. Budker, D. DeMille, D.F.J. Kimball, A. Derevianko, C.W. Clark, ArXiv e-prints, 2017, arXiv:1710.01833 [physics.atom-ph].
[28] C.A.J. O'Hare, A.M. Green, Phys. Rev. D 95 (2017) 063017, arXiv:1701.03118.

[29] W. Chung, Proceedings of the 39th International Conference on High Energy Physics, ICHEP2018, July 2018, Seoul, Korea, pp. 609.
[30] J.D. Jackson, Classical Electrodynamics, Third Edition, Wiley-VCH, 1998, pp. 832.
[31] J. Hong, J.E. Kim, S. Nam, Y. Semertzidis, ArXiv e-prints, 2014, arXiv: 1403.1576 [hep-ph].
[32] Y. Kahn, B.R. Safdi, J. Thaler, Phys. Rev. Lett. 117 (2016) 141801, arXiv: 1602.01086 [hep-ph].